Full Paper

Wiley Online Library

ELECTROANALYSIS

DOI: 10.1002/elan.201900690

MVF Sensor Enables Analysis of Nucleic Acids with Stable Secondary Structures

Marcos V. Foguel,[a] Angelica M. Balcarcel,[a] Mark A. Reed,[a] Percy Calvo-Marzal,[a] Yulia V. Gerasimova,[a] Dmitry M. Kolpashchikov,[a, b] and Karin Y. Chumbimuni-Torres*[a]

Abstract: One major challenge in nucleic acids analysis by hybridization probes is a compromise between the probe's tight binding and sequence-selective recognition of nucleic acid targets folded into stable secondary structures. We have been developing a four-way junction (4WJ)-based sensor that consists of a universal stem-loop (USL) probe immobilized on an electrode surface and two adaptor strands (M and F). The sensor was shown to be highly selective towards single base mismatches at room temperature, able to detect multiple targets using the same USL probe, and have improved ability to detect folded nucleic acids. However, some nucleic acid targets, including natural RNA, are folded into very stable secondary and tertiary structures, which may represent a challenge even for the 4WJ sensors. This work describes a new sensor, named MVF since it uses three probe stands M, V and F, which further improves the performance of 4WJ sensors with folded targets. The MVF sensor interrogating a 16S rRNA NASBA amplicon with calculated folding energy of −32.82 kcal/mol has demonstrated 2.5-fold improvement in a signal-to-background ratio in comparison with a 4WJ sensor lacking strand V. The proposed design can be used as a general strategy in the analysis of folded nucleic acids including natural RNA.

Keywords: Sensors, electrochemistry · nucleic acid · four-way junction · E. coli

1 Introduction

Electrochemical sensors based on nucleic acid recognition have received significant attention due to simplicity in their preparation and target detection [1–2]. Nucleic acid-assisted recognition followed by electron transfer to a gold surface allows for the electrochemical detection of various targets including specific DNA and RNA sequences [1,3–5]. First sensor designs that took advantage of this pathway utilized a stem-loop folded probe immobilized to the electrode's surface via a thiol group at one of its termini, while a redox marker was attached to the opposite probe terminus (Scheme 1A) [6]. The target hybridized to the loop portion of the probe thereby triggering opening of the stem-loop and removing the redox marker away from the electrode's surface [6–7]. This design exhibits an "ON-OFF" signal, i.e., the response is suppressed with the increasing target concentration [6–9]. Although this sensor design is widely used, it presents a number of significant limitations. First, stem-loop folded probes have limited selectivity, since they do not differentiate single nucleotide substitutions (SNS) at room temperatures (~22 °C) [9,10]. Second, being folded themselves, such probes are unable to efficiently interrogate single-stranded DNA or RNA folded in stable secondary structures [11,12]. Third, a new probe must be designed and attached to the gold electrode for each new target. Moreover, the "ON-OFF" signal operational mode of this design reduces the linear dynamic range of the target recognition [8].

Some of the challenges demonstrated by a simple stem-loop probe for electrochemical nucleic acid detection were overcome in the case of the three-way junction (3WJ) [10–11]. This design allowed the response to increase with the target concentration ("OFF-ON" signal), since it utilized an additional redox marker-containing strand, which was complementary to both the stem-loop probe and the target. Thus, the target triggered formation of the 3WJ structure with the stem-loop and additional strand, in which the redox marker was brought close to the electrode's surface, resulting in a current density signal proportional to the target concentration (Scheme 1B) [10–11]. However, the selectivity of the 3WJ design still did not allow discrimination of SNS, since it was still stable when an unpaired nucleotide was present [12]. In addition, the stem-loop strand was still complementary to the target, and so was needed to be re-designed, along with the second strand, every time a new nucleic acid sequence was analyzed.

[a] M. V. Foguel, A. M. Balcarcel, M. A. Reed, P. Calvo-Marzal, Y. V. Gerasimova, D. M. Kolpashchikov, K. Y. Chumbimuni-Torres
Department of Chemistry, University of Central Florida, 4000 Central Florida Blvd., Orlando, FL 32816, United States
E-mail: Karin.ChumbimuniTorres@ucf.edu
[b] D. M. Kolpashchikov
Burnett School of Biomedical Science, University of Central Florida, 4000 Central Florida Blvd., Orlando, FL 32816, United States

Supporting information for this article is available on the WWW under https://doi.org/10.1002/elan.201900690

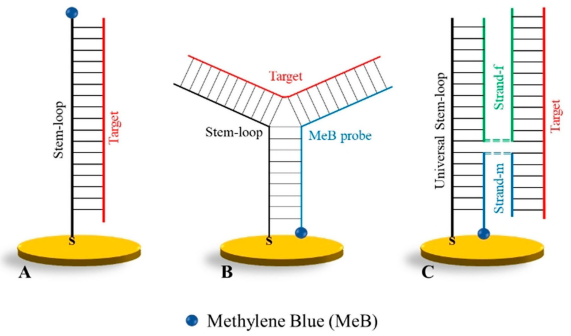

Scheme 1. Different designs of electrochemical nucleic acid sensors hybridized to a specific nucleic acid target: (A) a stem-loop probe labeled with a redox marker (MeB) is opened up by the target's presence; (B) the target triggers formation of a 3WJ structure by binding to the stem-loop and MeB-containing strands; and (C) a 4WJ structure is formed between the stem-loop, two adaptor strands, one of which contains the MeB redox marker, and the target.

We have been developing a DNA four-way junction (4WJ) platform that promises to advance electrochemical nucleic acid analysis [13–16]. The 4WJ is comprised of a universal stem loop (USL) strand, and two adaptor strands M and F, one of which is equipped with a redox marker (e.g. methylene blue, MeB). When strands M and F specifically bind to the adjacent positions of a nucleic acid target, they open USL and form a 4WJ structure, which positions MeB close to the electrode surface (Scheme 1C) [17]. The USL strand is universal in this design and does not need to be tailored to the target under analysis. Strand F is responsible for unwinding and tight binding to the target due to a relatively long target-binding arm [15,18–20], while strand M has a shorter target-binding arm (8–12 nt). Therefore, strand M is responsible for maintaining high selectivity of the target recognition by the 4WJ platform, since an SNS-containing target does not hybridize to strand M, thereby preventing formation of the 4WJ structure [13–16,21]. Furthermore, the 4WJ sensor enables the "OFF-ON" detection mode, as the target's presence brings the redox marker close to the electrode's surface [17]. Even though the reported 4WJ design allows for target unwinding due to higher affinity of strand F to the target, it is not very efficient in interrogating very stable target secondary structures, since it would require significant elongation in the target-binding arm of strand F, which would increase the likelihood of folding of strand F itself into a stem-loop structure and, thus, complicate its interaction with the target [13,22–23].

In this work, we developed an advanced 4WJ electrochemical sensor (MVF 4WJ) that combines the advantages of high selectivity and tight binding to analysed nucleic acids and further improves the ability of the sensor to interrogate highly structured nucleic acids. We demonstrated the ability of the MVF sensor to unwind targets corresponding to fragments of the *rrs* genes of a pathogenic *E. coli* O157:H7 strain and non-pathogenic *E. coli* K12 substrain MG1655. The new sensor exhibited an improved efficiency of interrogation of a fragment of 16S rRNA amplified using nucleic acid sequence-based amplification (NASBA) reaction, as compared with a conventional 4WJ electrochemical sensor. [17,20–21] This was achieved by incorporation of an additional target-unwinding strand (called here strand V, thereby giving the name to the sensor). Such modification in the conventional 4WJ design broadens the sensor application for nucleic acid analysis by allowing efficient binding to RNA targets with complex secondary structure.

2 Experimental

2.1 Chemicals

Oligonucleotides including the USL probe, strands F and V, synthetic targets and primers were purchased from Integrated DNA Technologies (Coralville, USA). Strand M oligonucleotides modified with a methylene blue (MeB) redox marker were obtained from Biosearch Technologies, Inc. (Petaluma, USA). The oligonucleotides were designed to minimize secondary structure using NUPACK analysis software [24]. The sequences are listed in Table 1, where the fragments for the targets were obtained by accession numbers U00096.3 and BA000007.2 for K12 and O157 *E. coli*, respectively. Tris(2-carboxyethyl) phosphine hydrochloride (TCEP), 6-mercapto-1-hexanol (MCH), trizma hydrochloride (Tris–HCl) and magnesium chloride were purchased from Sigma Aldrich (St. Louis, USA). Sulfuric acid, sodium hydroxide and sodium chloride were obtained from Fisher Scientific (Pittsburgh, USA). Saturated phenol at pH 4.3 (Sigma Life Sciences) and RNase-DNase chloroform:isoamyl alcohol (Acros Organics) were combined in 25:24:1 ratio for use in acidic phenol:chloroform extractions. RNase-DNase chloroform:isoamyl alcohol (Acros Organics) was used for chloroform back extractions. Alumina slurry (1.0 μm, 0.3 μm and 0.05 μm) was obtained from Buehler (Lake Bluff, USA). Gel Red was purchased from Biotium (Fremont, USA). The immobilization buffer (IB) was prepared with 50 mM Tris–HCl and 250 mM NaCl, the pH was adjusted to 7.4 using 1.0 M NaOH. The hybridization buffer (HB) was prepared with 50 mM Tris–HCl, 100 mM NaCl and 50 mM $MgCl_2$ and adjusted to pH 7.4 using 1.0 M NaOH. For NASBA reactions and amplicon isolation, non-DEPC (diethyl pyrocarbonate) treated RNase-free water (Boston BioProducts Inc.) was used. All other solutions were prepared with deionized water (18.2 MΩcm) using a Siemens PURELAB Ultra system (Lowell, USA).

2.2 NASBA

NASBA reactions were performed using a NASBA kit (Life Sciences Advanced Technologies, Inc. St. Petersburg, FL), 1 μM primers (Table 1) and 4 μg/μL *E. coli* 16S

Table 1. Oligonucleotides sequences* used in 4WJ-based sensor and NASBA.

Oligonucleotide	Sequence (5′–3′)
USL probe	/ThiolMC6–D/TTTTTTTTTTCGCGTTAACATACAATAGATCGCG
Strand F	GATCTATTG/iSp9/GCTGACGAGTGGCGGACGGGTG
Strand M K12	TTGCTGCTTC/iSp9/TATGTTAACTTTTTTTTTT–MeB
Strand M O157	AAGCTTGCTTCTTT/iSp9/TATGTTAACTTTTTTTTTT–MeB
Strand V1	GGTAACAGGAAG
Strand V2	GGTAACAGGAAGAAAAAAAAAA
Strand V3	GGTAACAGGAAG/iSp9/AAAAAAAAAA
K12 DNA	TGCGGTATTAGCTACCGTTTCCAGTAGTTATCCCCCTCCATCAGGCAGCTTCCCAGACATTACT
	CACCCGTCCGCCACTCGTCAGCGAAGCAGCAAGCTGCTTCCTGTTACCGTTCGACTTGCA
O157 DNA	TGCGGTATTAGCTACCGTTTCCAGTAGTTATCCCTCCATCAGGCAGTTTCCCAGACATTACT
	CACCCGTCCGCCACTCGTCAGCAAAGAAGCAAGCTTCTTCCTGTTACCGTTCGACTTGCA
Forward primer	AATTCTAATACGACTCACTATAGGGAAGAGGTTGCGACGTTATGCGGTATTAGCTA
Reverse primer	TGCAAGTCGAACGGTAACAGGA
NASBA	UUGCGACGUUAUGCGGUAUUAGCUACCGUUUCCAGUAGUUAUCCCCCUCCAUCAGGCAGUUUCCCAG
amplicon (K12 RNA)	ACAUUACUCACCCGUCCGCCACUCGUCAGCGAAGCAGCAAGCUGCUUCCUGUUACCGUUCGACUUGCA

*ThiolMC6-D: 5′ Thiol Modifier C6 S-S; MeB: Methylene Blue; iSp9: Triethylene glycol linker. Fragments of the probes/targets complementary to each other are color coded.

rRNA obtained by *in vitro* transcription (see Supporting Information). The final volume of each reaction mixture was 20 µL with amplification time of 90 min. The reaction conditions were used as specified by the vendor. NASBA reaction mixtures were diluted to 250 µL with RNase-free water, and RNA was extracted twice using acidic phenol:chloroform (1:1 v/v) according to a standard protocol. A chloroform:isoamyl back extraction (1:1 volume recovered RNA:solvent) was used to remove excess phenol, and the RNA product was ethanol-precipitated. Purified RNA was analyzed via gel electrophoresis in a 2 % w/v agarose gel containing 1 × Gel Red using 1 × TAE. Agarose gels were visualized using a BioRad Gel Doc XR+ system and Image Lab software (Figure S1). Concentrations of the purified RNA were approximated in gel using a reference band of a similar length in an RNA ladder (RiboRuler Low Range RNA ladder, Fisher Scientific, Pittsburgh, PA). Purification of RNA was confirmed using 260:280 nm absorbance ratios, and agarose gel electrophoresis.

2.3 Sensor Preparation

Gold disc electrodes (GDE) were cleaned by immersion in piranha solution (1:3 ratio of 30 % H_2O_2–98 % H_2SO_4) for 10 min and manually polished on a microcloth with an alumina slurry (1.0 µm, 0.3 µm and 0.05 µm). The GDEs were sonicated in water and ethanol for 2 min to remove residual alumina particles trapped on the electrode surface. Then, the GDE activation was performed by cyclic voltammetry in 0.5 M H_2SO_4 from 1.6 to −0.1 V at 100 mV/s and this step was used to determine the electroactive area of each electrode [25].

For USL immobilization on GDE surface, 1 mM TCEP was used to reduce the disulfide bond of the USL by shaking the solution for 1 h. This solution was diluted to 0.1 µM in IB and drop-casted (15 µL) on to GDEs for 30 min. Then, the GDEs were rinsed with IB and dried with nitrogen. Subsequently, 2 mM MCH (15 µL) was drop-casted and incubated for 30 min to reduce non-specific adsorption. The GDEs were rinsed with IB and dried with nitrogen. Afterward, hybridization was performed by dilution of the targets (K12, O157 and NASBA amplicon) to 50 nM in HB and addition of appropriate adaptors strands (M and F) and strand V (V1, V2 and V3) at desired concentrations. 15 µL of this solution was drop-casted onto the GDEs and incubated for 90 min. All the steps were performed at room temperature.

2.4 Electrochemical Measurements

Electrochemical measurements were performed in a CHI660D Electrochemical Workstation (CH Instruments, Austin, USA) with a conventional electrochemical cell composed of three electrodes: modified gold disc electrodes, Ag/AgCl (1 M KCl) and platinum wire as working, reference and counter electrodes, respectively. All electrodes were purchased from CH Instruments (Austin,

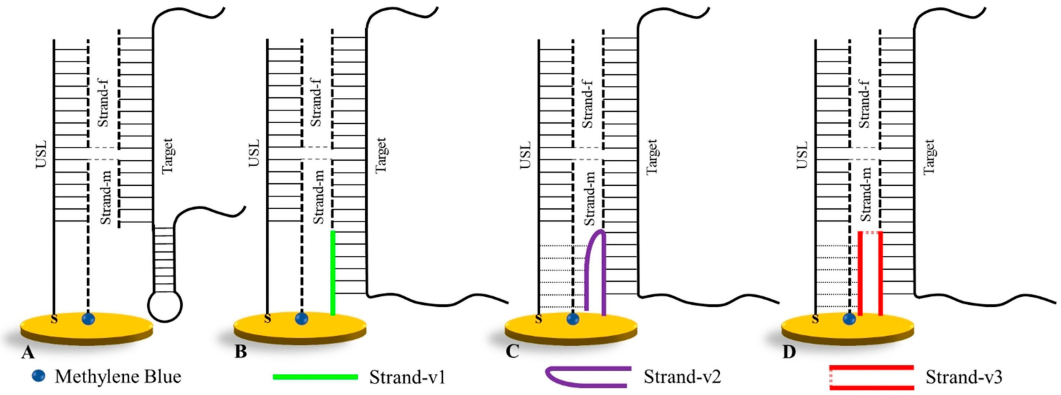

Scheme 2. Scheme of the 4WJ sensor in the absence of strand V (A) and in the presence of strand V1 (B), V2 (C) or V3 (D).

USA). Square wave voltammetry (SWV) was recorded from 0 to −0.5 V at a frequency of 100 Hz, amplitude of 70 mV and increment potential of 3 mV in HB solution at room temperature. Nitrogen was bubbled for 10 min into electrochemical cell to remove oxygen before the measurements. Each experiment was performed in triplicate (three separate working electrodes) to acquire statistically significant data.

3 Results and Discussion

3.1 Selection of the MVF Sensor Design

The design of the MVF sensor was based on the 4WJ sensor design reported by us earlier [17,26–28]. To improve the sensor's ability to interrogate highly structured RNA targets, we incorporated strand V in addition to strands M and F in the sensor design (Scheme 2). We explored three different variations of strand V: (i) a single-stranded oligonucleotide V1 hybridizing to a target fragment next to strand M (Scheme 2B); (ii) oligonucleotide V2 containing the same target-binding fragment as V1 elongated with an oligoA sequence that could hybridize with an oligoT "tails" of either USL or strand M for further stabilization of the 4WJ structure on the electrode's surface (Scheme 2C); (iii) oligonucleotide V3 containing the same nucleotide sequence as V2, but with the target-binding and oligoA fragments separated via a triethylene glycol linker for flexibility of strand V3/target/USL or strand V3/target/strand M interactions (Scheme 2D).

As targets, we used a fragment of 16S rDNA/RNA from E. *coli*. First, different MVF sensor designs were tested using a synthetic DNA target corresponding to a fragment of the *rrs* gene from *E. coli* K12 strain (K12 DNA). The best design was then used to interrogate other two targets: O157 DNA and K12 RNA (the latter was obtained by the NASBA reaction using *E. coli* 16S rRNA transcript). The targets folded into stable secondary structures, as predicted by M-fold software (Figure S2). A conventional 4WJ sensor was designed by making strand M complementary to a fragment of the DNA target containing two SNS in O157 DNA in comparison with K12 DNAs: a C > A substitution in the middle of strand M-target complex, and a G > A substitution in the end of the complex (Figure S2, panels A and B). The target's fragment interrogated by strand M was folded in a stem-loop structure. Therefore, strand F of the 4WJ sensor was designed complementary to a less structured fragment of the target next to strand M, including a stem portion of the stem-loop structure, to assist unwinding the stem. In the MVF 4WJ sensor design, an additional strand V was designed to interact with the target's fragment on the other side of strand M. The fragment of the target complementary to strand V included another stem portion of the stem-loop structure, as well as a less structured fragment of the target next to it. Therefore, binding of strand V to the target would stabilize the complex of the target with strands M and F. The performance of three different MVF 4WJ sensors was compared with each other and with that of the conventional 4WJ sensor containing the same strands M and F in the absence of strand V to demonstrate whether strand V contributes to unwinding of the target's secondary structure.

SWV measurements were carried out to compare the response of the three MVF sensor designs – MVF1, MVF2, and MVF3 containing strands V1, V2 and V3, respectively – with that of the 4WJ probe containing only strands M and F (Figure 1). We used K12 *E. coli* -specific sensor comprised of strands F and M–K12 in the presence and absence (blank) of K12 DNA target. The conventional 4WJ sensor (Scheme 2A) produced a current density peak of about 10.9 μA/cm^2 in the presence of the target (Figure 1A), which represents a 4-fold increase in the signal as compared to the blank response (compare red and blue curves), demonstrating that the 4WJ structure was successfully formed. The small signal observed for the blank could indicate that the methylene blue-containing strand M binds to the electrode's surface even in the absence of the target. Addition of strand V1 decreased the blank signal by ~30 %, possibly because of the increased local DNA concentration next to the

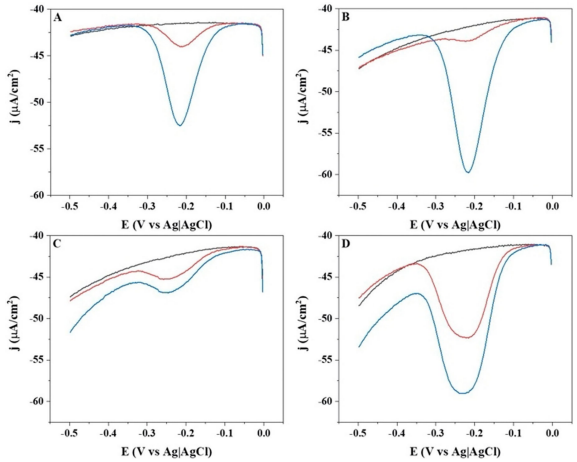

Fig. 1. SWV response after immobilization of USL probe, backfilling and hybridization with 0.5 μM strand F, 0.25 μM strand M-K12 and 50 nM K12 DNA in the absence of strand V (A) and in the presence of 0.5 μM strands V1 (B), V2 (C) or V3 (D). Black lines indicate baseline signal (GDE/USL/MCH); red lines indicate the blank response (all components, except for the target); and blue lines indicate signal after hybridization with the target.

electrode's surface that prevented the non-specific absorption of strand M (compare black and red curves in Figure 1B).

Upon addition of strand V1 (Figure 1B), the target-triggered signal exhibited ~15-fold increase with respect to the blank (17.3 μA/cm^2 vs 1.08 μA/cm^2), which was a significant improvement in comparison with the V-lacking 4WJ sensor. This indicates that V1 binds to the target and unwinds its secondary structure, thus stabilizing both the strand M/target complex and the entire 4WJ complex. Therefore, addition of strand V1 opens a possibility to detect lower concentrations of the target.

Elongation of strand V1 with an oligoA tail to promote its interaction with the oligoT fragments of USL and/or strand M did not improve the MVF sensor performance, as was observed for V1. In the case of strand V2-containing sensor (Figure 1C), the target did not cause significant increase of the current density peak (4.3 μA/cm^2) in comparison to the blank (3.0 μA/cm^2). We hypothesize that formation of a rigid double-stranded strand V-target and strand V-USL structures compromised interaction of the target-binding fragments of strands M and F with the USL probe, thus preventing formation of a stable 4WJ associate on the surface of the electrode. When a flexible triethylene glycol linker was introduced between oligoA and the target-binding fragment of strand V (as in the case of MVF-3 sensor), the target-induced formation of the 4WJ structure resulted in an intense current density peak of 17.3 μA/cm^2 (Figure 1D, blue curve), similarly to that observed for MVF-1. At the same time, the blank signal increased to 10.5 μA/cm^2 (Figure 1D, red curve), thus significantly compromising the overall signal-to-background ratio. This high response for the blank can be explained by the formation of a stable USL-strand V3 complex, which can further stabilize the target-independent M/F/V3/USL complex.

Interestingly, both the blank and the signal in the presence of K12 DNA target were higher for V3 than for V2 adaptor strands (compare Figure 1C and D). This is remarkable given that V3 differs from V2 by only the presence of a triethylene glycol linker (iSp9), which separates the oligoadenylate fragment (A^{10}) from the analyte binding arm (Table 1). Importantly, both V2 and V3 can form DNA triplex complexes with T^{10} fragments of USL probe and M strand. The data indicate that the flexible iSp9 linker enables greater stability of the quaternary complex M/F/V3/USL. We speculate that separation of a DNA fragment (target binding arm) from the rest of the complex by long and flexible linker reduces the repulsion of the negatively charged DNA and favors the complex formation.

Therefore, out of three sensor designs utilizing strand V for improved target interrogation, MVF1 was the only design exhibiting improved performance in the case of a long (124 nt) and highly structured target. Therefore, MVF1 sensor was chosen for further experiments.

3.2 Optimization of the MVF Sensor

First, concentrations of the adaptor strands M and F for the K12 sensor were optimized in the absence of strand V1. The sensor performance was evaluated based on the signal-to-background ratio (S/B), as shown in Table 2. As expected, the S/B values increased with the increase of strand F concentration when the concentration of strand M was set to 0.10 μM. In the case of higher strand M concentration (0.25 μM) the best S/B value was obtained in the presence of 1 μM strand F. For both trial 3 (0.1 μM strand M and 2.0 μM strand F) and trial 5 (0.25 μM strand M and 1.0 strand F), the S/B of 8 was achieved. However,

Table 2. Current density peak (expressed as the signal difference from the baseline) for different concentrations of the adaptor strands (M and F) using K12 DNA synthetic target.

Trial	M (μM)	F (μM)	K12 DNA (nM)	J_p[a] (μA/cm^2)	S/B[b]
1	0.1	0.5	0	1.4 ± 0.3	6.7
			50	9.6 ± 0.6	
2		1.0	0	0.9 ± 0.3	7.5
			50	7.1 ± 0.5	
3		2.0	0	0.70 ± 0.04	8.0
			50	5.6 ± 0.5	
4	0.25	0.5	0	2.1 ± 0.2	5.7
			50	11 ± 1	
5		1.0	0	1.5 ± 0.3	8.0
			50	11.7 ± 0.1	
6		2.0	0	2.07 ± 0.02	4.1
			50	8.4 ± 0.2	

[a] J_p = current density peak calculated as the baseline current signal minus the current signal for a sample; [b] S/B = signal-to-background ratio.

trial 3 suffered from a somewhat low current density in presence of the target, and trial 5 had slightly elevated signal for the blank. Thus, choosing one of these conditions could impair sensor performance. For this reason, further optimization experiments were performed using the conditions of trial 2 (0.1 μM strand M and 1.0 μM strand F), which resulted in a comparable S/B of 7.5 caused by low blank and a higher target-induced signal than for trial 3.

We then varied the concentration of strand V1 and tested the response of the MVF1 sensors specific for K12 (Figure 2a) and O157 (Figure 2b) using their complementary targets. It should be noted that for both sensors the same strand V1 was used, since it was complementary to both O157 and K12 *E. coli* strains (Figure S2, panels A and B).

The increased current density for the K12 sensor was observed with the increase of strand V1 concentration (Figure 2a). Using 2.0 μM strand V1, the signal intensity was 55 % higher than the signal obtained without strand V1, which highlights advantageous properties of strand V1 in unwinding the secondary structure of K12 DNA. A calibration curve was built for K12 sensors using synthetic K12 DNA in the presence and absence of strand V (data not shown). The linear range for both the 4WJ and MVF1 sensors was from 1 to 75 nM, however ~2.5-fold improvement in the limit of detection (LOD) was observed when strand V was used (the LOD of 1.02 nM and 0.43 nM was calculated using the 3σ rule for the conventional 4WJ sensor and MVF1 sensor, respectively).

The current density peak for the O157-specific MVF1 sensor increased slightly as the strand V1 concentration was increased (Figure 2b). However, the improvement of the signal using 2.0 μM strand V1 was only 10 % in comparison with the assay in the absence of strand V1. The difference in the strand V1 effect can be explained by the difference in the stability of the target secondary structures. When the stability is relatively low, strand F alone can efficiently unwind the target, so strand V1 does not contribute significantly. Nevertheless, for a stronger secondary structure, strand V1 plays an important role in assisting in the hybridization of the target to the sensor platform. As can be seen in Figure S2, the secondary structure of O157 DNA is less stable than that of K12 DNA (the predicted free energy values are −15.37 kcal/mol and −18.89 kcal/mol, respectively), which corroborates with the results presented in Figure 2.

Since a higher current density was observed at 2.0 μM of strand V1, this was the concentration used for further experiments.

3.3 Effect of Strand V1 on Interrogation of Long Targets with Stable Secondary Structures

As we observed that the effect of strand V1 relied on the free energy of the target secondary structure, the sensor was analyzed using K12 RNA containing the sensor-interrogated sequence. The RNA target was obtained by the NASBA reaction using *E. coli* 16S rRNA transcript as a template. The free energy for this amplicon was also predicted using M-fold, and the predicted value was −32.82 kcal/mol (Figure S2C), which indicated more stable secondary structure of K12 RNA than that of K12 DNA. Thus, we expected even more pronounced effect of strand V1 on the performance of the K12-specific MVF sensor in the presence of K12 RNA.

The effect of strand V1 was compared for the three targets (O157 DNA, K12 DNA and K12 RNA) using the respective sensors, and the results are shown in Figure 3.

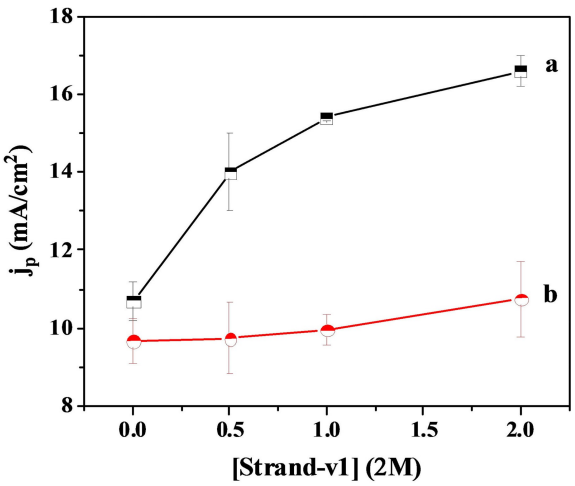

Fig. 2. Response of K12-(a) and O157-specific (b) MVF1 sensors to their complementary DNA targets in the presence of different concentrations of strand V1 (0.5, 1.0 and 2.0 μM); concentrations for strands M and F were 0.1 μM and 1.0 μM, respectively. j_p is current density peak calculated as the current signal for a sample minus the current for the baseline.

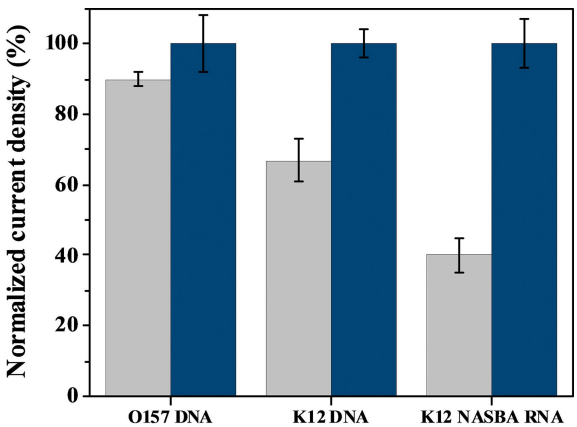

Fig. 3. Response of the 4WJ-based sensors designed to interrogate their complementary targets (O157 DNA, K12 DNA, or K12 RNA). Component concentrations: 0.10 μM strand M, 1.0 μM strand F, 2.0 μM strand V1, and 50 nM of target. The signal for the MVF1 sensors containing strand V1 (blue bars) was set to 100 %. The signal in the absence of strand V1 (grey bars) was normalized with respect to the signal in the presence of V1.

To make it easier to compare the results for different sensors, the average response of each sensor in the presence of V1 was set as 100 %, and the signal in the absence of V1 was normalized to its respective 100 % value.

The secondary structure of O157 DNA target is the least stable (−15.37 kcal/mol) among the targets evaluated, thus the presence of strand V1 increased the current density intensity by only 10 %. Therefore, the 4WJ platform composed of only the adaptor strands M and F is efficient enough to interrogate the targets with a relatively weak secondary structure. In contrast, K12 DNA target induced a 33 % higher signal with the addition of strand V1, which matches with the intermediate value for the free energy of the target (−18.89 kcal/mol) obtained by M-fold. Finally, the most pronounced effect of strand V1 on the efficiency of the target interrogation was observed for K12 RNA, as can be expected taking into account the lowest free energy predicted for this target. Therefore, in the case of highly structured targets (such as natural RNA, for example), addition of strand V1 can significantly enhance the performance of the 4WJ sensor by assisting in unwinding the target's secondary structure and promoting interaction of other sensor components with the target.

4 Conclusion

The 4WJ sensor shows high efficiency of the detection of long nucleic acid targets with stable secondary structures. However, for some targets folded into very stable intramolecular structures, the performance of the 4WJ sensors may be compromised due to less efficient interrogation of the target with the two strands of the sensor. This work demonstrated that such limitation can be overcome by the addition of an extra strand complementary to the target, called strand V. With the help from strand V and the synergistic interaction of strands V, F and M with the target, improved interrogation of the highly structured target can be achieved, with a clear correlation between the stability of the target's intramolecular structure and the effect of strand V addition. Such approach can benefit the analysis of RNA targets, which are known to exhibit stable secondary and/or tertiary structures.

Acknowledgements

The authors acknowledge NSF-CBET grant number #1706802 and Florida Health Department grant #7ZK05 and #7ZK33.

References

[1] J. Wang, G. Rivas, X. Cai, E. Palecek, P. Nielsen, H. Shiraishi, N. Dontha, D. Luo, C. Parrado, M. Chicharro, P. A. M. Farias, F. S. Valera, D. H. Grant, M. Ozsoz, M. N. Flair, *Anal. Chim. Acta* **1997**, *347*, 1–8.
[2] J. Zhai, H. Cui, R. Yang, *Biotechnol. Adv.* **1997**, *15*, 43–58.
[3] B. Khalilzadeh, M. Rashidi, A. Soleimanian, H. Tajalli, G. S. Kanberoglu, B. Baradaran, M. R. Rashidi, *Int. J. Biol. Macromol.* **2019**, *134*, 695–703.
[4] G. S. Santos, R. Caldas, F. L. Melo, I. S. Bruscky, M. A. L. Silva, L. B. Wanderley, C. A. S. Andrade, M. D. L. Oliveira, *Talanta* **2019**, *204*, 395–401.
[5] L. F. Garcia-Melo, I. Álvarez-González, E. Madrigal-Bujaidar, E. O. Madrigal-Santillán, J. A. Morales-González, R. N. Pineda Cruces, J. A. Campoy Ramírez, P. D. Matsumura, M. D. L. A. Aguilar-Santamaría, N. Batina, *J. Electroanal. Chem.* **2019**, *840*, 93–100.
[6] C. Fan, K. W. Plaxco, A. J. Heeger, *Proc. Natl. Acad. Sci. USA* **2003**, *100*, 9134–9137.
[7] Y. Xiao, R. Y. Lai, K. W. Plaxco, *Nat. Protoc.* **2007**, *2*, 2875–2880.
[8] L. Kekedy-Nagy, S. Shipovskov, E. E. Ferapontova, *Anal. Chem.* **2016**, *88*, 7984–7990.
[9] R. Ziółkowski, S. Oszwałdowski, K. Zacharczuk, A. A. Zasada, E. Malinowska, *J. Electrochem. Soc.* **2018**, *165*, B187-B195.
[10] S. Liu, W. Wei, T. Liu, L. Wang, *Chem. Asian J.* **2015**, *10*, 1903–1908.
[11] L. Feng, C. Zhao, Y. Xiao, L. Wu, J. Ren, X. Qu, *Chem. Commun. (Camb.)* **2012**, *48*, 6900–6902.
[12] J. L. Kadrmas, A. J. Ravin, N. B. Leontis, *Nucleic Acids Res.* **1995**, *23*, 2212–2222.
[13] D. M. Kolpashchikov, *J. Am. Chem. Soc.* **2006**, *128*, 10625–10628.
[14] C. Nguyen, J. Grimes, Y. V. Gerasimova, D. M. Kolpashchikov, *Chemistry* **2011**, *17*, 13052–13058.
[15] J. Grimes, Y. V. Gerasimova, D. M. Kolpashchikov, *Angew. Chem. Int. Ed. Engl.* **2010**, *49*, 8950–8953.
[16] Y. V. Gerasimova, A. Hayson, J. Ballantyne, D. M. Kolpashchikov, *ChemBioChem* **2010**, *11*, 1762–1768.
[17] D. M. Mills, P. Calvo-Marzal, J. M. Pinzon, S. Armas, D. M. Kolpashchikov, K. Y. Chumbimuni-Torres, *Electroanalysis* **2017**, *29*, 873–879.
[18] Y. V. Gerasimova, D. M. Kolpashchikov, *Biosens. Bioelectron.* **2013**, *41*, 386–390.
[19] M. Labib, S. M. Ghobadloo, N. Khan, D. M. Kolpashchikov, M. V. Berezovski, *Anal. Chem.* **2013**, *85*, 9422–9427.
[20] M. Labib, N. Khan, M. V. Berezovski, *Anal. Chem.* **2015**, *87*, 1395–1403.
[21] D. M. Kolpashchikov, *Chem. Rev.* **2010**, *110*, 4709–4723.
[22] D. M. Kolpashchikov, *J. Am. Chem. Soc.* **2005**, *127*, 12442–12443.
[23] N. Kikuchi, D. M. Kolpashchikov, *ChemBioChem* **2016**, *17*, 1589–1592.
[24] R. M. Dirks, J. S. Bois, J. M. Schaeffer, E. Winfree, N. A. Pierce, *SIAM Rev.* **2007**, *49*, 65–88.
[25] R. F. Carvalhal, R. Sanches Freire, L. T. Kubota, *Electroanalysis* **2005**, *17*, 1251–1259.
[26] D. M. Mills, M. V. Foguel, C. P. Martin, T. T. Trieu, O. Kamar, P. Calvo-Marzal, D. M. Kolpashchikov, K. Y. Chumbimuni-Torres, *Sens. Actuators B* **2019**, *293*, 11–15.
[27] C. A. Lynch, 3rd, M. V. Foguel, A. J. Reed, A. M. Balcarcel, P. Calvo-Marzal, Y. V. Gerasimova, K. Y. Chumbimuni-Torres, *Anal. Chem.* **2019**, *91*, 13458–13464.
[28] D. M. Mills, C. P. Martin, S. M. Armas, P. Calvo-Marzal, D. M. Kolpashchikov, K. Y. Chumbimuni-Torres, *Biosens. Bioelectron.* **2018**, *109*, 35–42.

Received: November 18, 2019
Accepted: January 12, 2020
Published online on January 27, 2020

